Volume 8
Number 10
14 March 2020
Pages 4965–5364

Journal of Materials Chemistry A

Materials for energy and sustainability

rsc.li/materials-a

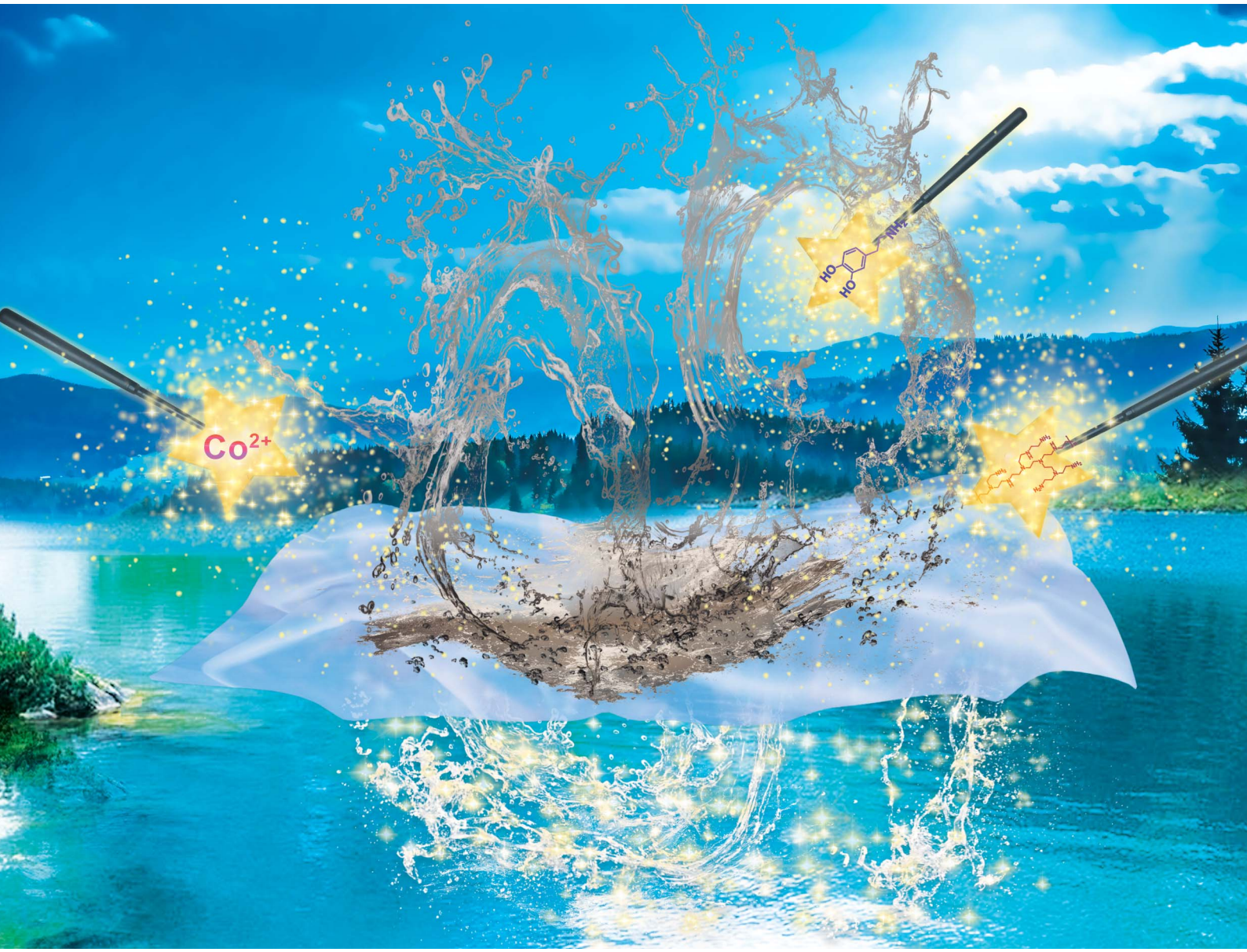

ISSN 2050-7488

ROYAL SOCIETY OF CHEMISTRY

PAPER

Lu Shao *et al.*

Ultra-thin trinity coating enabled by competitive reactions for unparalleled molecular separation

Journal of Materials Chemistry A

ROYAL SOCIETY OF CHEMISTRY

PAPER

View Article Online
View Journal | View Issue

Cite this: J. Mater. Chem. A, 2020, 8, 5078

Ultra-thin trinity coating enabled by competitive reactions for unparalleled molecular separation†

Yanqiu Zhang,[a] Jun Ma [b] and Lu Shao *[a]

Advanced nanoporous membranes with outstanding permeance and exceptional molecular-separation efficiency are highly desirable for key industrial applications for alleviating the worldwide environmental/energy crisis. Herein, an ultra-thin trinity coating (~33 nm) for unparalleled molecular separation is first built *via* covalent bond (CB)/coordination bond (COB) competitive reactions. The COBs generated among various polyphenols (PPhs), amino substances (ASs) and transition metal ions (TMIs) can limit Michael addition or Schiff base reactions for CB formation between PPhs and ASs during the mussel-inspired ternary coating process so as to elegantly engineer the trinity coating architecture on the porous substrate with ultra-thin thickness, excellent structural integration, high hydrophilicity and outstanding smoothness. Our molecular separation nanoporous membrane demonstrates ultra-high permeance (114 L m^{-2} h^{-1} bar^{-1} for Bromothymol Blue (BTB) and 104 L m^{-2} h^{-1} bar^{-1} for Congo Red (CR)) with complete rejection, which is much superior to that of state-of-the-art membranes and can realize the lower energy consumption of the membrane separation process. The CB/COB competitive reactions drastically enhanced the permeance of the trinity coated membrane by 533%, 238%, and 93% compared to that of the unary (pDA) and binary (pDA/PEI or pDA/Co^{2+}) coated membranes. Meanwhile, the novel membrane with the perfectly tuned architecture by CB/COB competitive reactions possesses extraordinary dye/salt selectivity, tremendous acid/alkali–base stability and excellent anti-pollution capacity simultaneously. The new strategy for building an outstanding trinity coating *via* competitive reactions can pave a realistic way for fabricating unparalleled next-generation separation membranes.

Received 19th November 2019
Accepted 7th January 2020

DOI: 10.1039/c9ta12670h

rsc.li/materials-a

Introduction

Membrane-based separation is growing in importance in liquid/gas purification and high-value substance recycling compared with traditional energy-intensive processes.[1–10] Although membrane separation can consume just 25% more than the minimum energy defined by thermodynamics, which is much less than that of traditional separation techniques like distillation (50 times more energy consumption than the thermodynamic limit), the limited flow rate requiring costly large plants hinders its widespread advanced application. Highly permeable membranes with excellent selectivity are desirable for large-scale separation processes considering the footprint in the stipulated time frame and much less energy being required at lower operating pressure, which can greatly alleviate the global water scarcity affecting ~4 billion people.[11,12] Highly permeable nanoporous membranes, especially for energetically efficient molecular-scale separations, require a precise selective layer for fast mass transportation and a suitable membrane–fluid interface. Therefore, a facile and versatile strategy for thin-film engineering is of particular interest to membrane scientists due to the selective-layer thickness down to the nanometer scale promoting transportation with less energy consumption.

Recent years have witnessed a rapidly growing interest in the formation of ultrathin membranes for energetically efficient molecular separations.[13–17] Although interfacial polymerization has been conducted with the aid of electro-spraying or sacrificial cadmium hydroxide nanostrands for ultrathin selective layer (nanofilm) fabrication, the environmental issues and process complexity of currently available methods greatly hinder their practical application.[1,18] Graphene-based materials can be simply filtered to form ultrathin membranes, achieving a pure water flux of 21.8 L m^{-2} h^{-1} bar^{-1} for dye molecule separations.[19] In fact, the stability of graphene-based ultrathin membranes is still a major issue because the hydrogen bonds between 2D layers for membrane formation can be readily deteriorated during aqueous environmental operation. In addition, the reliable performance of such ultrathin membranes prepared using 2D materials should be further improved and verified. Therefore, simplicity and compatibility

[a]MIIT Key Laboratory of Critical Materials Technology for New Energy Conversion and Storage, State Key Laboratory of Urban Water Resource and Environment, School of Chemistry and Chemical Engineering, Harbin Institute of Technology, Harbin 150001, China. E-mail: shaolu@hit.edu.cn

[b]State Key Laboratory of Urban Water Resource and Environment, School of Environment, Harbin Institute of Technology, Harbin, 150090, China

† Electronic supplementary information (ESI) available. See DOI: 10.1039/c9ta12670h

with large-scale production are the most important considerations for ultrathin membrane fabrication, for which surface coating seems the most viable method.[20] In addition, membrane stability should mainly be focused on because a small interference in the thin selective layer down to the nano scale may induce a huge "butterfly effect" on membrane performance when designing the nano-scale coating for thin-film engineering.

Phenolic compounds, more than 8000 kinds, are widely distributed in nature and constitute a major class of phytochemicals.[21–24] Currently, polyphenol-based surface coating as a simple, versatile, and tunable method to form a 100–1000 nm thick film has been developed for various applications such as drug release, anti-corrosion, and membrane separation, which demonstrates improved water permeance and selectivity.[25–36] However, there still remains a trade-off relationship between the selective layer thickness and the nanofiltration performance of membranes derived from phenolic compounds. Mussel-inspired unary polyphenol coating generates nanoporous membranes with thick selective layers and high mass transfer resistance because a longer coating time is required to avoid defects and poor separation performance due to polyphenol self-polymerization characteristics. Although binary polyphenol coating was utilized for a shorter coating time and tuned selective layers,[27,32,33] these membranes still demonstrate ordinary permeance due to the thick selective layer formed by the additional crosslinkers (polyphenols/amino substances) or have serious stability issues (polyphenols/metal ions) due to the lack of structural integrity. Therefore, it is still a great challenge to construct ultra-thin, defect-free, stable and fouling-resistant membranes for precise molecular separation.

Herein, inspired by the competition-driven evolution in nature such as for organismal complexity expansion,[37–39] the covalent bond (CB) and coordination bond (COB) competitive reactions among polyphenols (PPhs), amino substances (ASs) and transition metal ions (TMIs) were conceived to construct an exceptional ultra-thin trinity coating on a polyacrylonitrile (PAN-H) support membrane (Fig. 1 and S1†). Such CB/COB competitive reactions during the ternary coating procedures can elegantly engineer a nanoporous membrane architecture to build a homogeneously ultra-thin (33 nm-thick) trinity coating, achieving ultrahigh permeance, excellent dye sieving ability, excellent anti-fouling ability and tremendous acid/alkali–base stability simultaneously. Systematic physicochemical characterization revealed the formation mechanism of the competitive reaction built coating, underlying the great performance enhancement of our novel membranes. Most importantly, the new strategy driven by competitive reactions can be adapted to industrial processes for next-generation membranes, realizing exceptional energetically efficient molecular separation towards sustainable environmental/energy remediation.

Results and discussion

The first-row transition metal ions with empty d-orbitals were mainly investigated for coupling with polyphenols and amino substances for building the trinity coating because such metal elements can accept electrons by hybridized orbitals to achieve a steady state of 16 or 18 electrons for stronger coordination bond (COB) formation. Co^{2+}, dopamine and multi-arylamino polyethylenimine (PEI) were tentatively used as a typical ternary coating system for CB/COB competitive reactions to generate the exceptional trinity coating. According to Fig. 2a, the ternary coated membrane demonstrates a several fold increase in water permeance along with higher dye rejection compared with unary and binary coated membranes. It should be noted that such extraordinary permeance achieved by our membrane with trinity coating is ~10 times higher than that of

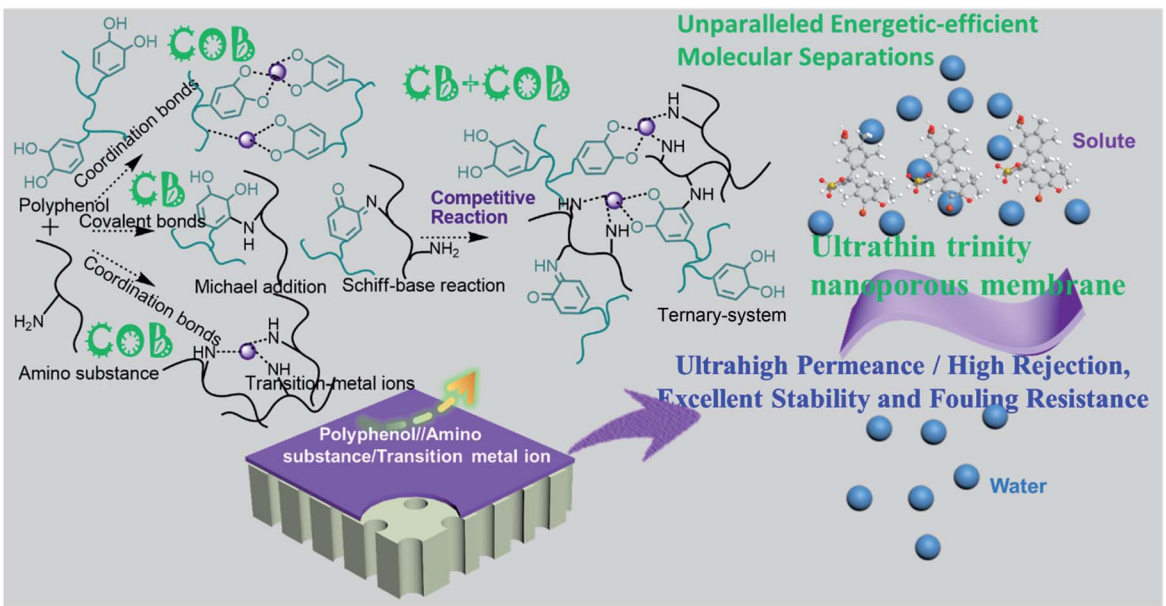

Fig. 1 The scheme of the fabrication process of the ultrathin trinity coating *via* CB/COB competitive reactions.

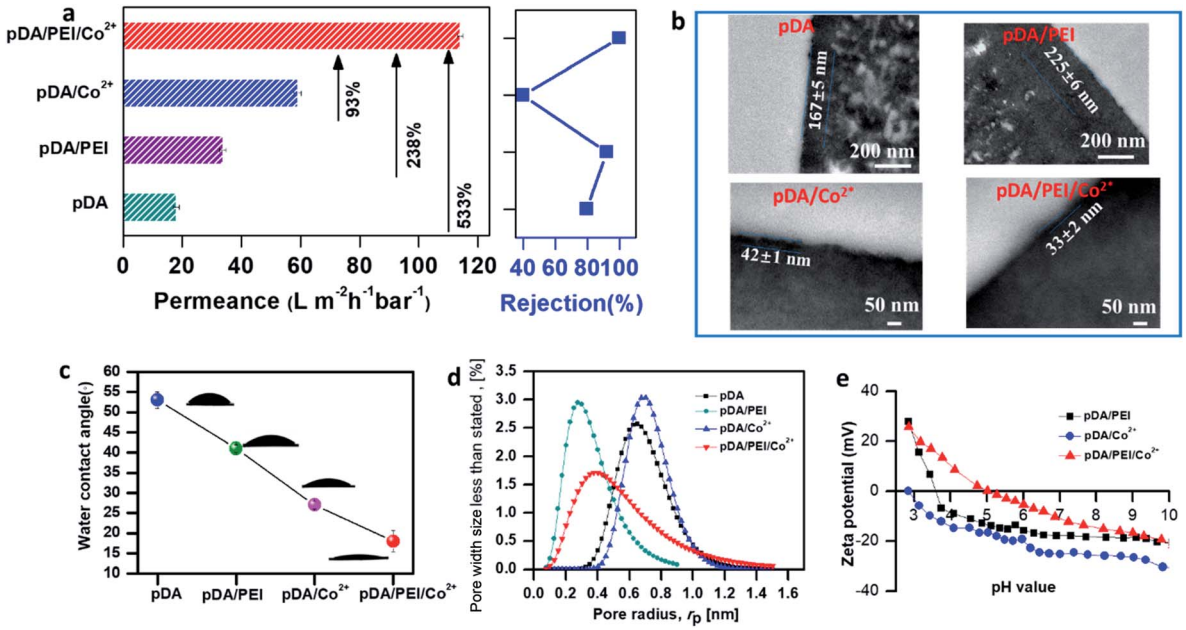

Fig. 2 (a) Permeance and (BTB) rejection results; (b) TEM images; (c) water contact angles (WCAs); (d) the pore size distribution; (e) zeta potentials of the binary (pDA/PEI and pDA/Co^{2+}) and ternary (pDA/PEI/Co^{2+}) coated membranes.

commercial membranes and much higher than that of state-of-the-art membranes with similar dye rejection.[40–44]

Various membranes with the unary, binary and ternary coatings were prepared to explore the architectural features which can greatly affect membrane separation performance. The TEM results illustrated (Fig. 2b) that the unary (pDA) and binary (pDA/PEI) coated layers have thicknesses of 167 nm and 225 nm, respectively. Correspondingly, numerous nano-structured papillae were present on the surface of the pDA and pDA/PEI coated membranes with relatively higher roughness (Fig. S2 and S3†). Dopamine (DA) oligomers can form pDA aggregates *via* non-covalent interactions, which were responsible for the highest roughness of the pDA coated membrane.[45–48] By introducing PEI into the pDA coating system, DA monomers can react with PEI (chains) *via* Michael addition or Schiff base reactions to construct a much thicker coating layer although the smoothness of the coating can be improved. Interestingly, greatly decreased thicknesses along with much smoother surfaces were observed in the pDA/Co^{2+} and pDA/PEI/Co^{2+} membranes. This was mainly because the coordination bonds during the coating can effectively interrupt the DA non-covalent interactions so as to limit pDA aggregate formation. In particular, the ternary coated membrane possessed the lowest thickness of ~33 nm and the lowest roughness of R_a = 1.64 nm (Fig. S3†), attributed to the CB/COB competitive reactions during pDA/PEI/Co^{2+} ternary coating. In addition, the ternary coated membrane possessed enhanced hydrophilicity compared to the unary (pDA) coated membranes or the binary coated membranes regulated only by covalent bonds (pDA/PEI) or coordination bonds (pDA/Co^{2+}) (Fig. 2c), which can be beneficial for water permeation and anti-fouling performance. Therefore, the ultrathin/hydrophilic trinity coating formed by CB/COB competitive reactions demonstrates an ultrahigh permeance of 114 L m^{-2} h^{-1} bar^{-1} with the complete rejection (~100%) of BTB (Fig. 2a). It should be noted that pDA/Co^{2+} has a much lower BTB rejection (40%) and less permeance (59 L m^{-2} h^{-1} bar^{-1}) although the pDA/Co^{2+} coated layer has comparable thickness and smoothness. The CB/COB competitive reactions drastically enhanced the permeance of the coated membrane by 533%, 238%, and 93% compared to the unary (pDA) and binary (pDA/PEI or pDA/Co^{2+}) coated membranes, and increased BTB rejection simultaneously. Furthermore, the pore size distributions (Fig. 2d) of various membranes were examined, which can confirm the unique advantages of our ultra-thin trinity coating because the ternary coated membrane had an optimized pore size distribution with smaller pore size for precise separations and wide distribution for higher permeance. The zeta potential results (Fig. 2e and S4†) indicated all coated membranes may have better rejection to anionic dyes.

Due to PEI's ability to interact with dopamine (*via* CBs) and metal ions (*via* COBs), the existence of PEI can regulate the competitive reactions of the coating system.[49–52] As shown in Fig. 3a, with the PEI concentration increasing from 0.2 wt% to 0.6 wt% in the ternary coating system, the BTB separation performance was significantly improved. This result was attributed to the fact that more PEI molecules were deposited on the substrate surface (N content increasing from 17.92% to 20.13% as shown in Table S1†) with a higher PEI concentration through the strong covalent reaction with pDA and the coordination reaction with Co^{2+}, leading to a membrane with fewer defects for precise molecular sieving. Simultaneously, the membranes were endowed with higher hydrophilicity when increasing the PEI content, beneficial for the permeance and anti-fouling performance (Fig. S5†).[53–55] However, when further

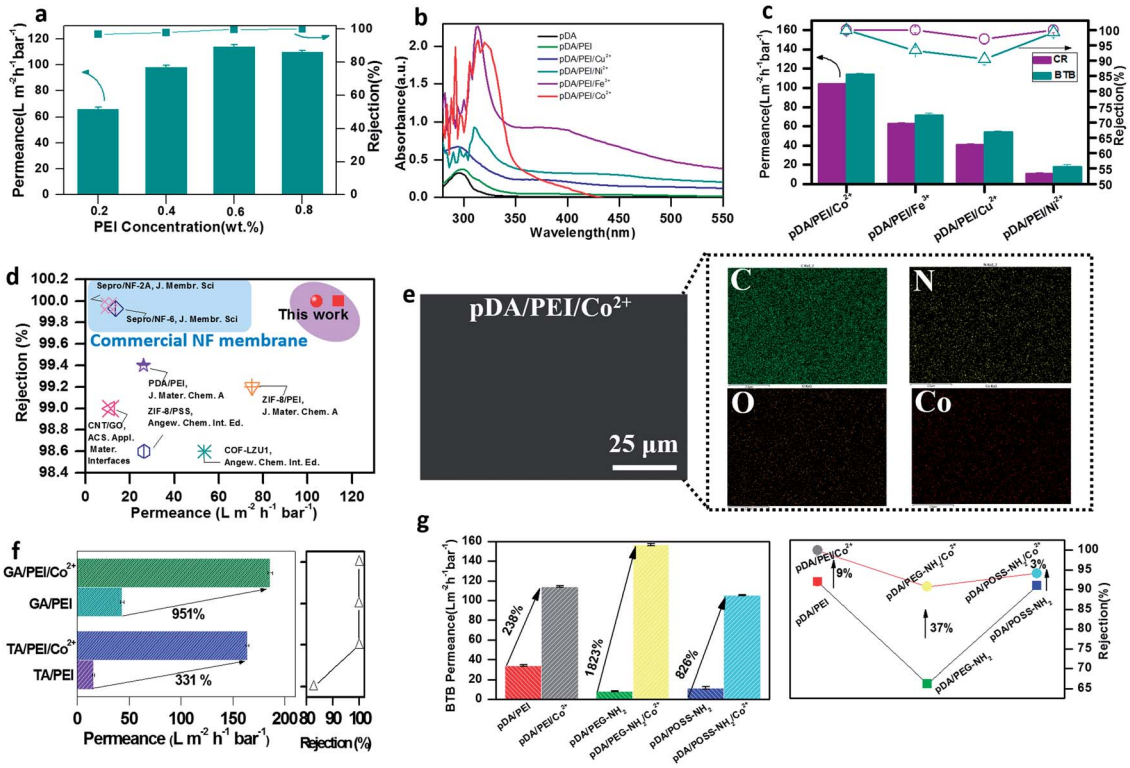

Fig. 3 (a) Permeance and rejection of the ternary coated membranes with different PEI concentrations; (b) UV-vis absorbance for various pDA/PEI/TMI solutions; (c) permeance and rejection of pDA/PEI/TMI coated membranes; (d) performance comparison of the pDA/PEI/Co^{2+} coated membrane with state-of-the-art membranes (red symbols represent the CR and BTB rejection, respectively); (e) SEM and EDX results of the pDA/PEI/Co^{2+} coated membrane; (f) permeance and rejection of GA/PEI, GA/PEI/Co^{2+}, TA/PEI, and TA/PEI/Co^{2+} membranes; (g) nanofiltration performance of ternary competitive pDA systems consisting of different structural ASs (linear polymer PEG-NH_2 and cage-like POSS-NH_2).

increasing the PEI content to 0.8 wt%, the excessive monomer might siege around the other monomers and react with dopamine or Co^{2+} to form oligomers rather than polymers,[56] which can diffuse into the pores of the selective layer resulting in the decline of permeance. Meanwhile, although increasing the PEI content can greatly reduce the defects of the trinity coating which is beneficial for higher rejection, the coating layer thickness would increase so as to boost the mass transfer resistance, resulting in a continuous decrease in permeance. Therefore, the optimum PEI concentration was fixed at 0.6 wt% for optimized dye rejection and permeance. Furthermore, the optimum ternary coating time was 6 h as shown in Fig. S6 and S7.†

In order to gain in-depth insight into the CB/COB competitive reaction effect, diverse TMIs (Fe^{3+}, Co^{2+}, Ni^{2+}, and Cu^{2+}) were also introduced into the ternary coating system. It should be noted that we chose Fe^{3+} instead of Fe^{2+} in the first-flow transitional series owing to the instability of Fe^{2+}. Based on the Irving and Williams rule the ionization potential and stability increase when the ionic radius decreases gradually. Therefore, the coordination capacity order of TMIs is $Fe^{3+} > Co^{2+} > Ni^{2+} > Cu^{2+}$.[57] For the dopamine involved ternary coating system, the special active phenolic hydroxyl and amino groups can not only form special COBs with the TMI, but also generate imide bonds during the polymerization process which also create stable COBs with TMI. Dopamine polymerization following the mechanism of radical polymerization requires oxidants. Therefore, Fe^{3+}, Ni^{2+} and Cu^{2+} as active catalysts can accelerate the polymerization of dopamine. Moreover, the addition of polyamines (PEI) can react with dopamine to form CB by Michael addition and Schiff base reaction. At the same time, PEI reacts with TMIs to form COBs. Thus, the formation process of COBs in such a ternary coating system is very interesting. To explain the conceivable mechanism of trinity coating formation, ultraviolet-visible (UV-vis) spectroscopy was utilized to characterize various coated membranes. Fig. 3b shows the UV-vis absorbance spectra of the pDA/PEI/TMI solution at 320 nm and 412 nm. The absorption peak at around 320 nm was associated with the formation of a Schiff base structure (C=C–C=N) from the pDA/PEI complex and the oxidation of dopamine, while the absorption peak at around 412 nm was attributed to the polymerization of dopamine (C=C–C=O). For the Fe^{3+}, Ni^{2+} and Cu^{2+} ternary coating systems, the absorbance at 412 nm was obviously higher than that of pDA/PEI and other pDA/PEI/TMI coating systems. Fe^{3+}, Ni^{2+} and Cu^{2+} are able to produce reactive oxygen species (ROS) in the solution, which can help to break through the oxygen diffusion gradient and boost dopamine oxidation.[58,59] To further verify the catalytic effect, Fe^{3+}, Ni^{2+} or Cu^{2+} ions were added into the pDA/PEI solution after polymerization for 4 h. Obviously, for Ni^{2+} and Cu^{2+}, the polymerization process was accelerated (Fig. S8†) and much thicker separating layers (>200 nm) were

formed (Fig. S9†), which result in low permeance (18 L m^{-2} h^{-1} bar^{-1} for pDA/PEI/Ni^{2+} and 56 L m^{-2} h^{-1} bar^{-1} for pDA/PEI/Cu^{2+}) due to the large mass transfer resistance (Fig. 3c). Different from that of Ni^{2+} and Cu^{2+}, the powerful coordination ability of Fe^{3+} with both PEI and dopamine can limit Michael addition or Schiff base reactions between dopamine and PEI, resulting in an ultra-thin selective layer (62 nm for pDA/PEI/Fe^{3+}) with the aid of strong COBs. This can be evidenced by the high absorbance at 298 nm which was attributed to the unpolymerized dopamine and its oxidation products (5,6-dihydroxyindole and pDA oligomers). Co^{2+} has very weak catalytic ability but asimilar coordination ability to Fe^{3+}, which forms the thinnest pDA/PEI/Co^{2+} trinity coating of ~33 nm. Therefore, the CB/COB competitive reactions during pDA/PEI/Co^{2+} ternary coating can well manipulate the coating structure, resulting in ultra-high permeance (114 L m^{-2} h^{-1} bar^{-1} for BTB and 104 L m^{-2} h^{-1} bar^{-1} for CR) and excellent dye rejection (~100%). In fact, the performance of our ternary coated membrane is unparalleled compared to state-of-the-art membranes for molecular separations (Fig. 3d and Table S2†).[28,40–44] Furthermore, XPS and FTIR spectroscopy results confirmed the successful trinity coating[60,61] (Fig. S10, S11 and Table S3†). The relative composition (ratio) of dopamine: AS unit: TMI (Fig. S12†) was also given for the ternary coated membrane. EDX analysis clearly demonstrated the uniform dispersion of metal ions and provided proof of the homogeneous coating as Fig. 3e and S13† show.

Most importantly, the ternary coating strategy *via* CB/COB competitive reactions can be extended to diverse polyphenols and amino substances besides various transition metal ions for building advanced trinity coatings. For example, gallic acid (GA) and tannic acid (TA) can also react with ASs to form CBs through Michael addition and Schiff base reactions due to their dopamine-like catechins. However, because of their different structural characteristics compared with those of dopamine, the elaborated membrane structures were different. The reaction of dopamine and PEI can form a large cross-linking network on the membrane surface because dopamine can aggregate to form large polymer chains. Compared with dopamine, there were more functional groups in GA (three phenolic hydroxyl groups and one carboxy group) that could react with PEI for introducing more PEI into the trinity coatings. During this process, GA was mainly involved in the formation of oligomers, which could react with PEI to form a dense network structure, resulting in an increased thickness of the selective layer of the membrane. It endowed the functional coatings with low permeance (<100 L m^{-2} h^{-1} bar^{-1}). Moreover, because TA has a certain acidity and has more phenolic hydroxyl groups, a large number of protons will be released when adding it into the solutions containing PEI, resulting in plenty of flocculants being formed, which might block the pores of the TA/PEI selective layer so as to decrease the membrane permeance. The addition of Co^{2+} reduced the formation of flocculants in the reaction due to the formation of COBs and made the membrane possess ultra-thin thickness (Fig. S14–S17†). As shown in Fig. 3f, adding Co^{2+} into GA/PEI or TA/PEI increased the membrane permeance by 951% and 331% while the retention rate remained unchanged. The superior nanofiltration performance of ternary coated membranes with different ASs was also verified[62] (Fig. 3g and S18–S24†).

Fig. 4a demonstrates the performance of the pDA/PEI/Co^{2+} ternary coated membrane for various dyes. The permeances of CR, RB, MB, BTB and CV were 104 L m^{-2} h^{-1} bar^{-1}, 21 L m^{-2} h^{-1} bar^{-1}, 37 L m^{-2} h^{-1} bar^{-1}, 114 L m^{-2} h^{-1} bar^{-1} and 121 L m^{-2} h^{-1} bar^{-1}, respectively. During nanofiltration of dye solutions, organic dye molecules used in the testing process will inevitably be adsorbed to some degree, but the process was relatively fast, only occurring in the initial period. Furthermore, quantitative adsorption tests of dyes on the ternary coated membrane were performed. After 30 min (Fig. S25†), the dye adsorption capacity remained stable, indicating that the dye adsorption had reached saturation. There was almost no adsorption of neutral BTB. The ultraviolet-visible absorption spectra of the feed and filtrate after 3 h were obtained, which proved that the nanofiltration membrane itself exhibited good separation performance not the adsorption (Fig. S26†). Excellent solute rejections of ternary coated membranes, attributed to both the Donnan effect and size exclusion effect, were demonstrated, which follow the order of CR(1.43 × 2.20 nm) = RB(1.54 × 1.20 nm) = MB(1.62 × 2.03 nm) = BTB(1.26 × 1.09 nm) (100%) > CV(1.31 × 1.31 nm) (70%). The fast adsorption in the initial period might influence the nanofiltration performance. CV, RB and MB underwent relatively higher adsorption than CR and BTB but they still belongs to the separation membrane. The membrane pores might be blocked, leading to low permeance and high rejection for RB and MB with a larger size and negative charge. The difference was that CV showed lower rejection and high permeance due to its small size and positive charge. In addition, the neutral dye BTB underwent almost no adsorption with the molecular size being larger than the membrane pore size, which accounted for high permeance and rejection. In general, the pore size of the membrane should be appropriately manipulated to alleviate the influence of the electrostatic attraction between the organic dyes and membrane surface for sufficient dye rejection. Due to the above reasons, we employed the neutral dye BTB to study the separation performance of the membrane. A long-term test up to 70 h illustrated the excellent stability of our ternary coated membrane (Fig. 4b). Meanwhile, the trinity coated nanofilm showed very low rejection for both monovalent and multivalent salts (18.1% for $MgCl_2$, 15.2% for $MgSO_4$, 13.3% for Na_2SO_4, and 4.0% for NaCl) (Fig. 4c). These results indicated that the ternary coated membrane exhibited typical separation behavior of loose-NF membranes with high dye rejection and low salt rejection because the membrane nanopore size was tuned delicately between the size of organic molecules and salt ions (Fig. 2d). In the context of resource conservation and sustainable development, membranes capable of fractionating salts and small organic molecules are essential for many applications. In fact, the membrane exhibited good selectivity for the separation of dyes from dye/salty water with an ultra-high permeability even at elevated salt concentrations (up to 3000 ppm) (Fig. 4d). The fouling behavior of our ternary coated membrane was also investigated and the results showed the flux recovery ratio (FRR) of BSA and HA for the cycling test was excellent under the conditions of complete dye rejection

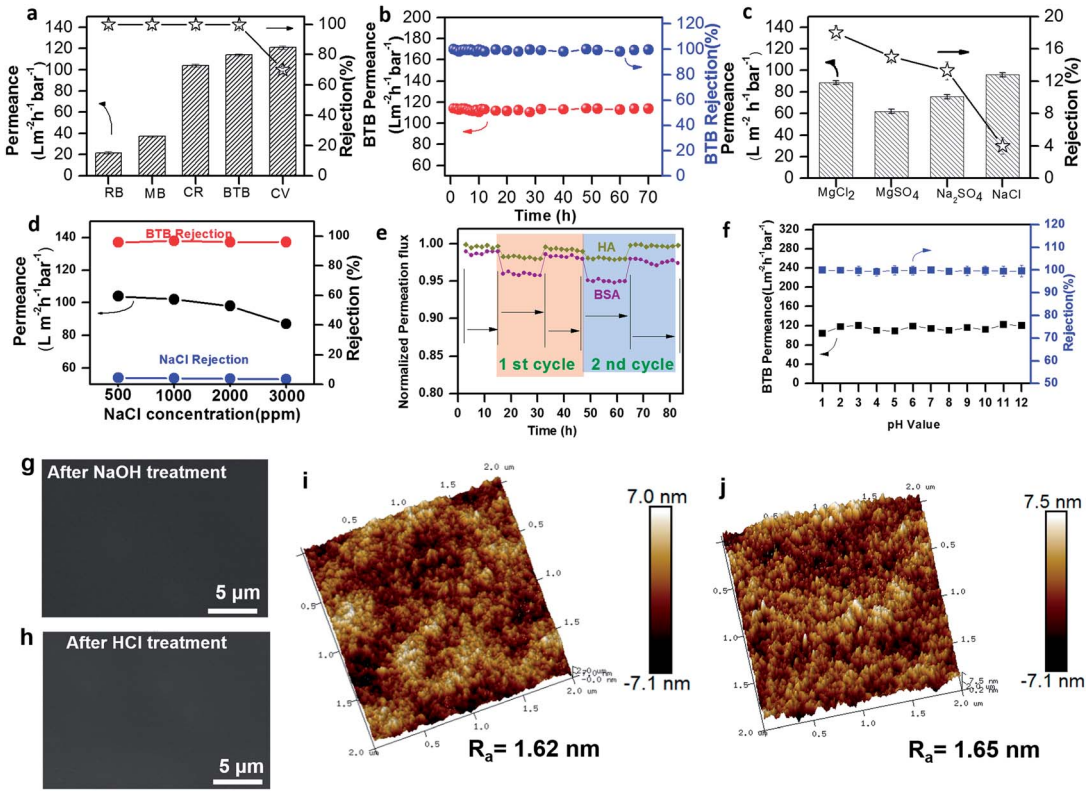

Fig. 4 (a) The different dye separation performances; (b) the time-dependent permeance; (c) the different salt separation performances; (d) the separation performance of dyes from dye/salty water; (e) normalized flux during the antifouling test (1 g L^{-1} BSA and 1 g L^{-1} HA); (f) effect of acidic and alkaline treatment on the performance of the pDA/PEI/Co^{2+} coated membrane; (g) SEM and AFM images after NaOH (0.05 M) (g and i) and HCl (0.05 M) (h and j) treatment for the pDA/PEI/Co^{2+} ternary coated membrane.

(Fig. 4e).[63–65] The excellent resistance towards hydrophobic biomolecules was due to the hydrophilic nature of the negatively charged ternary coated membrane, which can reduce the hydrophobic interaction between the hydrophobic BSA/HA molecule and the membrane coated surface and enhance the membrane anti-fouling ability. The membrane structural stability is more important for practical applications. The concentration of TMIs in the filtrate was determined by Inductively Coupled Plasma Mass Spectrometry (ICP-MS). No ions were detected (Table S5†). This demonstrated that secondary pollution of water will not be caused by the novel membrane. Besides, we also treated the membrane with an acid and an alkali for 24 h and no obvious change in nanofiltration performance was observed (Fig. 4f). The surface states of the pDA/PEI/Co^{2+} membrane were further measured by SEM, AFM and XPS after acid/alkali-base treatment (Fig. 4g–j and Table S6†). The surface structure and element content of the membrane were maintained before and after treatment too. These results strongly proved the excellent acid/alkali stability of our ternary coated membrane manipulated by the CB/COB competitive reaction.

Conclusions

In summary, covalent bond (CB)/coordination bond (COB) competitive reactions as a universal toolbox were utilized to modulate the coating architecture during ternary coating on porous substrates for constructing unparalleled energetically efficient molecular separation membranes. The ternary coated membrane possessed an ultra-thin layer, higher hydrophilicity and better surface smoothness, validating the ultra-high permeance, excellent dye/salt selectivity, tremendous acid/alkali stability and excellent anti-fouling ability. This work can facilitate the rapid development of next-generation molecular separation membranes *via* rational coating reaction design, and the new ternary coating strategy can also be applied to build a novel coating layer with controlled properties for diverse applications such as drug delivery and anti-corrosion.

Conflicts of interest

There are no conflicts to declare.

Acknowledgements

This work was supported by the National Natural Science Foundation of China (21878062).

Notes and references

1 M. R. Chowdhury, J. Steffes, B. D. Huey and J. R. McCutcheon, *Science*, 2018, **361**, 682–686.

2 Z. Tan, S. Chen, X. Peng, L. Zhang and C. Gao, *Science*, 2018, **360**, 518–521.
3 M. F. Jimenez-Solomon, Q. Song, K. E. Jelfs, M. Munoz-Ibanez and A. G. Livingston, *Nat. Mater.*, 2016, **15**, 760–767.
4 Z. Y. Wang, Z. G. Wang, S. H. Lin, H. L. Jin, S. J. Gao, Y. Z. Zhu and J. Jin, *Nat. Commun.*, 2018, **9**, 2004.
5 J. T. Liu, D. Hua, Y. Zhang, S. Japip and T. S. Thung, *Adv. Mater.*, 2018, **30**, 1705933.
6 X. Q. Cheng, Z. X. Wang, X. Jiang, T. Li, C. H. Lau, Z. Guo, J. Ma and L. Shao, *Prog. Mater. Sci.*, 2018, **92**, 258–283.
7 X. Wang, C. Chi, K. Zhang, Y. Qian, K. M. Gupta, Z. Kang, J. Jiang and D. Zhao, *Nat. Commun.*, 2017, **8**, 14460.
8 Z. Ali, F. Pacheco, E. Litwiller, Y. Wang, Y. Han and I. Pinnau, *J. Mater. Chem. A*, 2018, **6**, 30–35.
9 B. Mi, *Science*, 2019, **364**, 1033–1034.
10 D. S. Sholl and R. P. Lively, *Nature*, 2016, **532**, 435–437.
11 S. Kim, X. Lin, R. Ou, H. Liu, X. Zhang, G. P. Simon, C. D. Easton and H. Wang, *J. Mater. Chem. A*, 2017, **5**, 1533–1540.
12 X. Jiang, S. He, S. Li, Y. Bai and L. Shao, *J. Mater. Chem. A*, 2019, **7**, 16704–16711.
13 M. A. Rahim, S. L. Kristufek, S. Pan, J. J. Richardson and F. Caruso, *Angew. Chem.*, 2019, **58**, 1904–1927.
14 S. Ling, Z. Qin, W. Huang, S. Cao, D. L. Kaplan and M. J. Buehler, *Sci. Adv.*, 2017, **3**, e1601939.
15 Z. Jiang, S. Karan and A. G. Livingston, *Adv. Mater.*, 2018, **30**, 1705973.
16 Q. Yang, Y. Su, C. Chi, C. T. Cherian, K. Huang, V. G. Kravets, F. C. Wang, J. C. Zhang, A. Pratt and A. N. Grigorenko, *Nat. Mater.*, 2017, **16**, 1198–1202.
17 N. C. Su, D. T. Sun, C. M. Beavers, D. K. Britt, W. L. Queen and J. J. Urban, *Energy Environ. Sci.*, 2016, **9**, 922–931.
18 S. Karan, Z. Jiang and A. G. Livingston, *Science*, 2015, **348**, 1347–1351.
19 Y. Han, Z. Xu and C. Gao, *Adv. Funct. Mater.*, 2013, **23**, 3693–3700.
20 R. Y. Han and P. Y. Wu, *J. Mater. Chem. A*, 2019, **7**, 6475–6481.
21 G. R. Beecher, *J. Nutr.*, 2003, **133**, 3248S.
22 J. Li, X. Li, L. Zeng, S. Fan, M. Zhang, W. Sun, X. Chen, M. O. Tadé and S. Liu, *Nanoscale*, 2019, **11**, 3877–3887.
23 X. Yang, L. Yan, J. Ma, Y. Bai and L. Shao, *J. Membr. Sci.*, 2019, **591**, 117353.
24 X. Yang, L. Yan, Y. Wu, Y. Liu and L. Shao, *J. Membr. Sci.*, 2019, **589**, 117223.
25 W. E. Bentley and G. F. Payne, *Science*, 2013, **341**, 136–137.
26 A. H. Hofman, I. A. van Hees, J. Yang and M. Kamperman, *Adv. Mater.*, 2018, **30**, e1704640.
27 S. Zhao and Z. Wang, *J. Membr. Sci.*, 2017, **524**, 214–224.
28 X. Q. Cheng, Z. X. Wang, J. Guo, J. Ma and L. Shao, *ACS Sustainable Chem. Eng.*, 2017, **6**, 1881–1890.
29 Y. Chen, L. Fu, W. Yi, H. Lin and H. Lei, *J. Membr. Sci.*, 2017, **537**, 407–415.
30 Y. Lv, H. C. Yang, H. Q. Liang, L. S. Wan and Z. K. Xu, *J. Membr. Sci.*, 2015, **476**, 50–58.
31 J. Wang, J. Y. Zhu, M. T. Tsehaye, J. Li, G. Y. Dong, S. S. Yuan, X. Li, Y. T. Zhang, J. D. Liu and B. V. D. Bart, *J. Mater. Chem. A*, 2017, **5**, 14847–14857.
32 R. Zhang, Y. Su, X. Zhao, Y. Li, J. Zhao and Z. Jiang, *J. Membr. Sci.*, 2014, **470**, 9–17.
33 H. Ejima, J. J. Richardson, K. Liang, J. P. Best, M. P. van Koeverden, G. K. Such, J. Cui and F. Caruso, *Science*, 2013, **341**, 154–157.
34 T. Chakrabarty, L. Pérez-Manríquez, P. Neelakanda and K.-V. Peinemann, *Sep. Purif. Technol.*, 2017, **184**, 188–194.
35 H. C. Yang, R. Z. Waldman, M.-B. Wu, J. Hou, L. Chen, S. B. Darling and Z.-K. Xu, *Adv. Funct. Mater.*, 2018, **28**, 1705327.
36 X. Jiang, S. Li, Y. Bai and L. Shao, *J. Mater. Chem. A*, 2019, **7**, 10898–10904.
37 K. Winkelmann, M. J. Genner, T. Takahashi and L. Rüber, *Nat. Commun.*, 2014, **5**, 3.
38 A. S. Thorpe, E. T. Aschehoug, D. Z. Atwater and R. M. Callaway, *J. Ecol.*, 2011, **99**, 729–740.
39 I. Ispolatov, E. Alekseeva and M. Doebeli, arXiv preprint arXiv:1902.05723, 2019.
40 H. G. Fan, J. H. Gu, H. Meng, A. Knebel and J. Caro, *Angew. Chem., Int. Ed.*, 2018, **57**, 4083–4087.
41 R. Zhang, S. Ji, N. Wang, L. Wang, G. Zhang and J. R. Li, *Angew. Chem.*, 2015, **126**, 9933–9937.
42 L. Yang, Z. Wang and J. Zhang, *J. Mater. Chem. A*, 2017, **5**, 15342–15355.
43 Y. Han, Y. Jiang and C. Gao, *ACS Appl. Mater. Interfaces*, 2015, **7**, 8147–8155.
44 J. Y. Lin, W. Y. Ye, H. M. Zeng, H. Yang, J. N. Shen, S. Darvishmanesh, P. Luis, A. Sotto and B. V. Bruggen, *J. Membr. Sci.*, 2015, **477**, 183–193.
45 H. C. Yang, K.-J. Liao, H. Huang, Q. Y. Wu, L. S. Wan and Z. K. Xu, *J. Mater. Chem. A*, 2014, **2**, 10225–10230.
46 J. Wang, W. Z. Lang, H. P. Xu, X. Zhang and Y.-J. Guo, *Chem. Eng. J.*, 2015, **260**, 90–98.
47 J. Zhu, A. Uliana, J. Wang, S. Yuan, J. Li, M. Tian, K. Simoens, A. Volodin, J. Lin, K. Bernaerts, Y. Zhang and B. Van der Bruggen, *J. Mater. Chem. A*, 2016, **4**, 13211–13222.
48 X. Li, C. Liu, W. Yin, T. H. Chong and R. Wang, *J. Membr. Sci.*, 2019, **584**, 309–323.
49 C. Z. Liang, S. P. Sun, F. Y. Li, Y. K. Ong and T. S. Chung, *J. Membr. Sci.*, 2014, **469**, 306–315.
50 L. Yang, Z. Wang and J. Zhang, *J. Membr. Sci.*, 2017, **532**, 76–86.
51 G. J. Zhang, M. Hong and S. L. Ji, *Desalination*, 2009, **242**, 313–324.
52 P. Li, Z. Wang, L. B. Yang, S. Zhao, P. Song and B. Khan, *J. Membr. Sci.*, 2018, **555**, 56–68.
53 K. J. Kim, G. Chowdhury and T. Matsuura, *J. Membr. Sci.*, 2000, **179**, 43–52.
54 J. Song, X. M. Li, Y. Zhang, Y. Yin, B. Zhao, C. Li, D. Kong and T. He, *J. Membr. Sci.*, 2014, **471**, 372–380.
55 Y. Zhou, S. H. Yu, C. J. Gao and X. S. Feng, *Sep. Purif. Technol.*, 2009, **66**, 287–294.
56 N. Uzal, N. Ates, S. Saki, Y. E. Bulbul and Y. S. Chen, *Sep. Purif. Technol.*, 2017, **187**, 118–126.
57 D. A. Johnson and P. G. Nelson, *Inorg. Chem.*, 1995, **34**, 5666–5671.

58 J. Zhu, J. Wang, A. A. Uliana, M. Tian, Y. Zhang, Y. Zhang, A. Volodin, K. Simoens, S. Yuan, J. Li, J. Lin, K. Bernaerts and B. Van der Bruggen, *ACS Appl. Mater. Interfaces*, 2017, **9**, 28990–29001.
59 C. Zhang, H. N. N. Li, Y. Du, M. Q. Ma and Z. K. Xu, *Langmuir*, 2017, **33**, 1210–1216.
60 X. B. Yang, Z. X. Wang and L. Shao, *J. Membr. Sci.*, 2018, **549**, 67–74.
61 Y. Q. Zhang, H. G. Sun, H. Sadam, Y. Y. Liu and L. Shao, *Chem. Eng. J.*, 2019, **371**, 535–543.
62 S. W. Li, X. Jiang, X. B. Yang, Y. P. Bai and L. Shao, *J. Membr. Sci.*, 2019, **570**, 278–285.
63 N. Meng, W. Zhao, E. Shamsaei, G. Wang, X. Zeng, X. Lin, T. Xu, H. Wang and X. Zhang, *J. Membr. Sci.*, 2018, **548**, 363–371.
64 H. G. Sun, Y. Q. Zhang, S. W. Li, Y. P. Bai, J. Ma and L. Shao, *ACS Appl. Mater. Interfaces*, 2019, **11**, 35501–35508.
65 S. N. Ramanan, N. Shahkaramipour, T. Tran, L. Zhu, S. R. Venna, C.-K. Lim, A. Singh, P. N. Prasad and H. Lin, *J. Membr. Sci.*, 2018, **554**, 164–174.